Naval Research Laboratory

Washington, DC 20375-5320

NRL/MR/6180--20-10,061

Structures of Fluorocarbon, Siloxane, and Hydrocarbon Surfactant Monolayers at Air-water and Heptane-water Interfaces by Molecular Dynamics Simulations

Xiaohong Zhuang
Katherine M. Hinnant
Ramagopal Ananth

Naval Technology Center for Safety and Survivability Branch
Chemistry Division

May 26, 2020

REPORT DOCUMENTATION PAGE

Form Approved
OMB No. 0704-0188

1. REPORT DATE *(DD-MM-YYYY)*	**2. REPORT TYPE**	**3. DATES COVERED** *(From - To)*
26-05-2020	NRL Memorandum Report	21-02-2017 – 20-02-2018

4. TITLE AND SUBTITLE

Structures of Fluorocarbon, Siloxane, and Hydrocarbon Surfactant Monolayers at Air-water and Heptane-water Interfaces by Molecular Dynamics Simulations

5a. CONTRACT NUMBER

5b. GRANT NUMBER

5c. PROGRAM ELEMENT NUMBER

6. AUTHOR(S)

Xiaonhong Zhuang, Katherine M. Hinnant, and Ramagopal Ananth

5d. PROJECT NUMBER

5e. TASK NUMBER

5f. WORK UNIT NUMBER
6A70/1P02

7. PERFORMING ORGANIZATION NAME(S) AND ADDRESS(ES)

Naval Research Laboratory
4555 Overlook Avenue, SW
Washington, DC 20375-5320

8. PERFORMING ORGANIZATION REPORT NUMBER

NRL/MR/6180--20-10,061

9. SPONSORING / MONITORING AGENCY NAME(S) AND ADDRESS(ES)

Office of Naval Research
One Liberty Center
875 N. Randolph Street, Suite 1425
Arlington, VA 22203-1995

10. SPONSOR / MONITOR'S ACRONYM(S)

ONR/SERDP

11. SPONSOR / MONITOR'S REPORT NUMBER(S)

12. DISTRIBUTION / AVAILABILITY STATEMENT

DISTRIBUTION STATEMENT A: Approved for public release; distribution is unlimited.

13. SUPPLEMENTARY NOTES

14. ABSTRACT

We predict interfacial structure and properties by performing molecular dynamics simulations of surfactant monolayers at air/water and heptane/water interfaces, and their interactions with fuel. The predicted values of surface area and surface tension agree reasonably well with experimental data and validate the methods including the CHARMM36 lipid force field. Moreover, the Gibbs elasticity of perfluorocarbon and siloxane surfactants at air-water interface are greater than the two hydrocarbon surfactants considered in this study. High Gibbs elasticity and low surface tension may suggest higher stability of bubble surfaces packed with the fluorocarbon and siloxane surfactants to dilatation of the lamellae than those with the hydrocarbon surfactants. The heptane penetration distance into the heptane-water interface is also smaller for the fluorocarbon and siloxane surfactants compared to the hydrocarbon surfactants.

15. SUBJECT TERMS

Fluorocarbon surfactants Fluorine-free surfactants Siloxane
Molecular dynamics Surface tension

16. SECURITY CLASSIFICATION OF:			**17. LIMITATION OF ABSTRACT**	**18. NUMBER OF PAGES**	**19a. NAME OF RESPONSIBLE PERSON**
a. REPORT	**b. ABSTRACT**	**c. THIS PAGE**			Ramagopal Ananth
Unclassified Unlimited	Unclassified Unlimited	Unclassified Unlimited	Unclassified Unlimited	32	**19b. TELEPHONE NUMBER** *(include area code)* (202) 767-3197

Standard Form 298 (Rev. 8-98)
Prescribed by ANSI Std. Z39.18

This page intentionally left blank.

CONTENTS

FIGURES

EXECUTIVE SUMMARY

Aqueous foams containing perfluorocarbon surfactants are used to suppress pool fires world-wide due to their unique interfacial properties. However, the spread of perfluorocarbons in the environment, bioaccumulation, and toxicity issues have raised many concerns. Therefore, we aim to study surfactant monolayers to facilitate the process of searching new surfactant in order to replace the toxic fluorocarbon surfactants contained in firefighting foams using molecular dynamics (MD) simulation. MD simulations mimic the physical movements of atoms (position and velocity) by numerically solving Newton's equations of motion subject to interatomic potentials (i.e. force field) on tens of nano-seconds scale. We developed experimentally validated MD models for a few examples of siloxane and hydrocarbon surfactants and developed an understanding of the differences with a fluorocarbon surfactant in air/water and heptane/water interfacial structures. The validated MD models can be used to develop new understanding of how variations in chemical structure impact interface structure and may give rise to new surfactant designs in future works.

Through MD simulations, we study the properties of surfactant monolayers at air/water and heptane/water interfaces that relate to the interfacial stability and the effects of fuel. We examine the interfacial properties of a few commercially available hydrocarbon (sodium dodecyl sulfate, SDS, and hexadecyltrimethylammonium bromide, CTAB (or C_{16}TAB)) and siloxane (2,2,4-trimethyl-4-[(trimethylsilyl)oxy]-3,8,11,14,17,20,23,26,29,32-decaoxa-2,4-disilatritrilacontane known as Silwet L77) surfactants and compare them with a commercial perfluorosurfactant (2,2,3,3,4,4,5,5,6,6,7,7,8,8,8-pentadecafluorooctanoic acid, PFOA). The simulation results demonstrate that the predicted values of surface area and surface tension agree reasonably well with experimental data and validate the methods including the CHARMM36 lipid force field used to simulate the surfactant molecules in foams. Moreover, the simulation results show that the Gibbs elasticity of perfluorocarbon and siloxane surfactants at air-water interface are greater than the two hydrocarbon surfactants considered in this study. High Gibbs elasticity and low surface tension may suggest higher stability of bubble surfaces packed with the fluorocarbon and siloxane surfactants to dilatation of the lamellae than those with the hydrocarbon surfactants. The heptane penetration distance into the heptane-water interface is also smaller for the fluorocarbon and siloxane surfactants compared to the two hydrocarbon surfactants.

This page intentionally left blank.

Structures of Fluorocarbon, Siloxane, and Hydrocarbon Surfactant Monolayers at Air-water and Heptane-water Interfaces by Molecular Dynamics Simulations

1. INTRODUCTION

Interfacial properties are important for generating aqueous foams that are effective in suppressing a pool fire. Foams are applied onto a liquid pool to cover the surface and block the fuel vapors feeding the fires. Foam stability plays a key role in maintaining the foam barrier on the pool surface leading to fire suppression. Foam stability depends on a variety of properties including surface tension, interface stability, and interactions with the fuel (e.g., heptane) pool. Aqueous foams containing perfluorocarbon surfactants are used to suppress pool fires world-wide due to their unique interfacial properties. However, the spread of perfluorocarbons in the environment, bioaccumulation, and toxicity issues have raised many concerns [1, 2]. Hydrocarbon and siloxane surfactants are being considered as potential replacements. Establishing relationships among changes in the chemical structures of a surfactant to the interfacial structures and properties can be used to design replacement surfactants with improved interfacial stability. In this paper, molecular dynamics (MD[1]) simulations are performed to understand the differences in surfactant interface properties stemming from the difference in interface structures among perfluorocarbon, hydrocarbon, and siloxane surfactants.

Despite using the same generation method, foams generated from perfluorocarbon surfactants have foam degradation, bubble coarsening, and liquid drainage rates significantly smaller than those generated from hydrocarbon surfactants [3-7]. Foam degradation caused by exposure to a liquid fuel pool is also significantly smaller for foams generated from perfluorocarbon surfactants than those generated from hydrocarbon surfactants [3]. The perfluorocarbon tail of a perfluorosurfactant is both oleo and hydro phobic unlike the tail of a hydrocarbon surfactant [8] and it is unclear to what extent the oleophobicity might affect the ability of fluorosurfactants to resist foam degradation by heptane. Surfactants adsorbed at a bubble surface and their interactions with water and heptane play a crucial role in influencing the stability of a bubble lamella by affecting both the interfacial stability and micelle properties [9].

We study the properties of surfactant monolayers at air/water and heptane/water interfaces that relate to the interfacial stability and the effects of fuel. We examine the interfacial properties of a few commercially available hydrocarbon (sodium dodecyl sulfate, SDS[2], and hexadecyltrimethylammonium bromide, CTAB[3] (or C_{16}TAB)) and siloxane (2,2,4-trimethyl-4-[(trimethylsilyl)oxy]-3,8,11,14,17,20,23,26,29,32-decaoxa-2,4-disilatritrilacontane known as

[1] MD: molecular dynamics
[2] SDS: sodium dodecyl sulfate
[3] CTAB: hexadecyltrimethylammonium bromide

Manuscript approved April 16, 2020.

Silwet L77[4]) surfactants and compare them with a commercial perfluorosurfactant (2,2,3,3,4,4,5,5,6,6,7,7,8,8,8-pentadecafluorooctanoic acid, PFOA[5]). The chemical structures of the surfactants are shown in **Figure 1**. The interfacial properties include surface and interfacial tensions, component density profiles, interfacial thickness, Gibbs elasticity, and zeta potential. We perform MD simulations of surfactant monolayers employing all-atom CHARMM36 lipid force field (C36FF[6]) [10] and TIP3P water model [11, 12] to predict differences in the interfacial properties among the different surfactants and compare the predictions with experimental data to validate the methods and the force field used in the simulations. The firefighting surfactants in this work are chosen partly because experimental data for the interfacial properties are available or can be measured. The hydrocarbon surfactants SDS and CTAB at an air-water interface were simulated using MD previously [13] and serve as references to compare against the siloxane and the fluorocarbon surfactants. A validated model can be used to understand the effects of surfactant's structural changes on interface and film stability in future works.

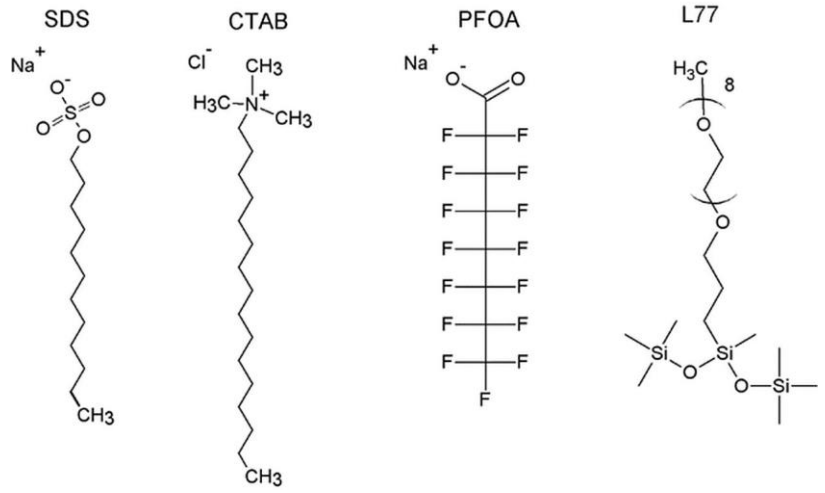

Fig. 1

The chemical structures of hydrocarbon surfactants SDS and CTAB, perfluorocarbon surfactant PFOA, and siloxane surfactant L77. For CTAB (or C_{16}TAB), as the parameter for the free bromide ion is not available in CHARMM force field, the bromide is replaced by chloride in our MD simulations.

MD simulations mimic the physical movements of atoms (position and velocity) by numerically solving Newton's equations of motion subject to interatomic potentials (i.e. force field) on tens of nano-seconds scale. Hydrocarbon surfactants (SDS and C_{14}TAB) surfactant monolayers were modeled and validated by experimental data previously. Gamba et al. [14] performed MD simulations of Newton black films with water molecules sandwiched between two monolayers of SDS and showed that the monolayer structures at hundreds of picoseconds to be

[4] L77: 2,2,4-trimethyl-4-[(trimethylsilyl)oxy]-3,8,11,14,17,20,23,26,29,32-decaoxa-2,4-disilatritrilacontane
[5] PFOA: 2,2,3,3,4,4,5,5,6,6,7,7,8,8,8-pentadecafluorooctanoic acid
[6] C36FF: CHARMM36 lipid force field

consistent with X-ray reflectivity data. Tarek et al. [15] performed MD simulations of tetradecyltrimethylammonium bromide (C_{14}TAB) monolayers at an air-water interface at two different concentrations (or areas per molecule) using CHARMM19 force field. They found that the predicted number density profiles normal to the interface were consistent with neutron reflectivity data. Chanda and Bandyopadhyay [16] considered a nonionic surfactant with an alkane tail and its interactions with an alkane fuel. They predicted number density profiles and molecular orientations of monolayers of monododecyl diethylenglycol ($C_mH_{2m+1}[OC_2H_{4n}]OH$) surfactants at air-water and decane-water interfaces. They found that the presence of decane increases the interface thickness due to interactions with the hydrocarbon tail of the surfactant. Watarai and Onoe [17] simulated surfactants at a heptane-water interface. They simulated the interfacial absorptivity of 2-hydroxy oximes attached to a nonyl group at a heptane-water interface and showed that the hydroxyoxime and nonyl groups stay in aqueous and heptane phases respectively. Zhang et al. [18] compared two surfactants with same head but with perfluorocarbon and hydrocarbon tails at an air-water interface. They performed MD simulations of oligo ethyleneoxide-2-perfluorooctyl monolayers and oligo ethyleneoxide-2-octyl surfactant monolayers at an air-water interface using CHARMM force field and showed that the fluorocarbon monolayer structure was more ordered than the hydrocarbon counterpart leading to a smaller surface tension. They also suggested that replacing one or two perfluorocarbons with hydrocarbons in the surfactant molecule did not influence the interfacial structure significantly. Stone et al. [19] simulated double tailed fluorinated phosphate (each tail is perfluorohexane-oxyethylene) and its hydrocarbon counterpart at a liquid CO_2-water interface and showed that both CO_2 and water penetrated hydrocarbon surfactant monolayers more than the fluorocarbon counterpart, which separated the CO_2 and water phases better. Pang and Xu [20] performed MD simulations of an air-water interface structure in the presence of surfactant mixtures and compared against the individual surfactants. They performed MD simulations of SDS, dodecyltrimethylammonium bromide (DTAB or C_{12}TAB), and octaethyleneglycol monododecyl ether ($C_{12}E_8$) by themselves and along with hydrocarbon, fluorocarbon, and siloxane co-surfactants. The co-surfactants were linear-polyethyleneoxide and branched-propylene oxide segments connected to a perfluoropentane, pentane, and silicone tail. The predictions showed that the highly ordered surfactant structures at the interface correlated with smaller measured surface tensions and $C_{12}E_8$/hydrocarbon co-surfactant system exhibiting the highest order. The co-surfactants contributed to more ordered structures relative to individual SDS, DTAB, and $C_{12}E_8$ surfactants. However, the silicone co-surfactant made the $C_{12}E_8$ structure more disordered and DTAB structure more ordered. These simulations showed that interactions between co-surfactants and fuel affect packing density and interfacial properties.

Mayo et al. [21] proposed DREIDING force field with a generic approach to simulating a novel combination of elements rather than a more specialized and accurate force field such as C36FF [10]. The C36FF is designed for proteins, nucleic acids, lipids, and small carbohydrates and is used in the current work. Using the DREIDING force field, Jang and Goddard [13] performed MD simulations of Newton black films of SDS and CTAB (or C_{16}TAB) and predicted the most probable surface concentration (or surface area) based on interface formation energy with packing density. Jang and Goddard [13] also calculated the structure, density profiles, disjoining pressure, Gibbs elasticity, shear modulus and yield strength of the films. Jang et al. [22] studied the effect of varying the position of the benzenesulfonate head group attached to a hexadecane backbone at a decane-water interface. Jang et al. [22] showed that the interfacial tension increased with decreasing interface thickness. The minimum interfacial tension and maximum interface

thickness values occurred when the benzenesulfonate head was attached at the fourth carbon position on the hexadecane backbone. Jang et al. [22] also inferred that the effective length of the alkane tail to be closest to the length of decane leading to increased miscibility and maximum interface thickness.

2. OBJECTIVE

Very few studies consider simulating monolayers of surfactants of interest to firefighting. To replace the toxic fluorocarbon surfactants contained in firefighting foams, new siloxane and hydrocarbon surfactants must be synthesized and characterized by themselves and in combination [23]. As a first step, we developed experimentally validated MD models for a few examples of siloxane and hydrocarbon surfactants and developed an understanding of the differences with a fluorocarbon surfactant in air/water and heptane/water interfacial structures. The validated MD models can be used to develop new understanding of how variations in chemical structure impact interface structure and may give rise to new surfactant designs in future works.

3. APPROACH

The MD simulations are performed on air-water and heptane-water interface systems with and without a surfactant, some of which are shown in **Figure 2**. A specified constant number of molecules, volume, and temperature (*NVT*[7]) ensemble was applied for the air-involved systems, such as air/water and air/surfactant-monolayer/water interfaces (**Figure 2b)**. Simulations with *NVT* ensemble predict positions and velocities of atoms, and pressure with time which are used to calculate surface tension and then Gibbs elasticity. A specified constant number of atoms, pressure, and temperature (*NPT*[8]) ensemble was applied for the systems not involving air, such as water, heptane, heptane/water and heptane/surfactant-monolayer/water interfaces (**Figure 2a and 2c)**. Simulations with *NPT* ensemble predict positions and velocities of atoms and volume with time which are used to calculate the densities of the pure water and heptane liquid, and also the interfacial properties related to surfactant packing such as area per molecule, component density, and interfacial thicknesses. More detail descriptions on each of the simulation system are provided in the subsection below.

[7] *NVT*: constant number of atoms, volume, and temperature
[8] *NPT*: constant number of atoms, pressure, and temperature

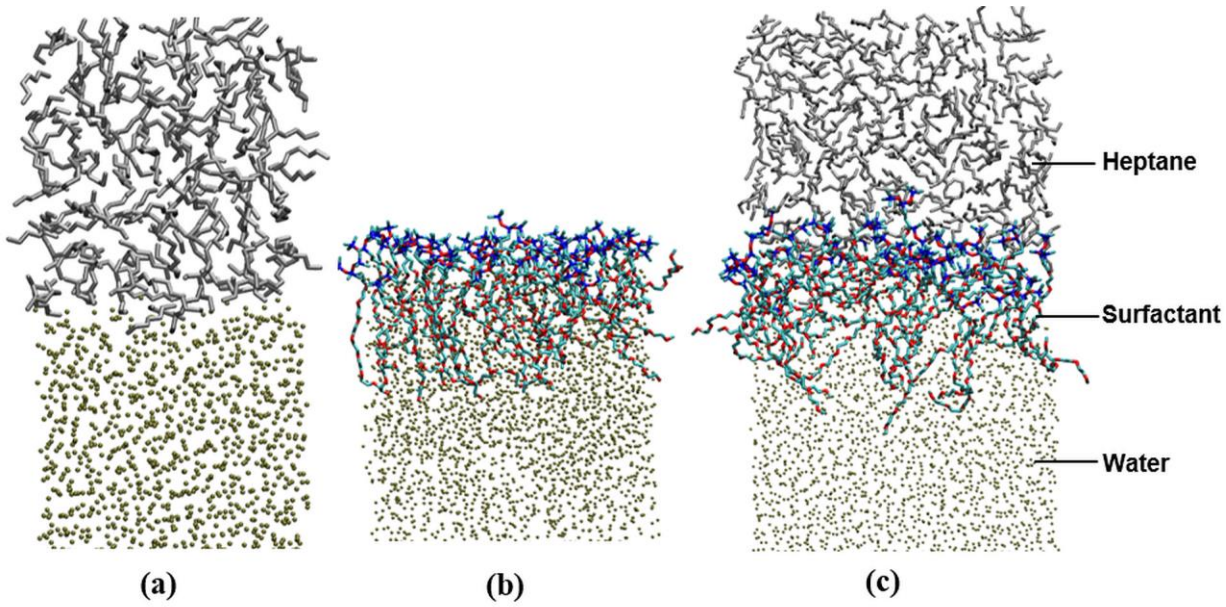

Fig. 2

The heptane/water, siloxane surfactant-monolayer/water, and heptane/siloxane surfactant-monolayer/water systems at the end of the MD simulations. Water is shown as tan spheres, heptane as silver lines. Siloxane surfactant L77, C, O, Si atoms are shown in cyan, red, and blue, respectively. Only the top half in the z direction of the simulation setup are shown, the bottom half is a mirror image of top.

Nanoscale Molecular dynamics (NAMD) computational program [24] was used to run the MD simulations. Chemistry at HARvard Macromolecular Mechanics (CHARMM) [25] was used to build the models and the property calculations. C36FF [10] was used for hydrocarbon and fluorocarbon surfactants, and also for heptane. CHARMM22 siloxane parameters [26] were used for the siloxane surfactant tail and C36FF [10] was used for the head group. TIP3P water model [11, 12] was applied. Periodic boundary conditions were applied to avoid edge artifacts and obtain good statistical data. To increase efficiency for van der Waals interactions, a switch function with a switch distance of 10.0 Å was applied so that the interaction was switched off 2.0 Å before the cut-off (12.0 Å). For the electrostatic interactions, the particle mesh Ewald summation was applied which splits the summation into short- and long-range interactions separated by the cut-off. The temperature was set at experimental temperatures. Langevin dynamics was applied to non-hydrogen atoms to maintain constant temperature with a Langevin coupling coefficient of 1.0 ps^{-1}. When *NPT* ensemble was applied, the pressure was set at 1.0 atm, and Nosé-Hoover Langevin-piston algorithm was used to maintain constant pressure with a piston period of 50.0 fs and a piston decay of 25.0 fs. Python modules NumPy and SciPy [27] were used for further data analyses. Visual Molecular Dynamics (VMD) [28] was applied to visualize and plot the simulated systems. Gnuplot [29] was used to plot the result data.

3.1 Pure Systems without Surfactant

Pure Water A cubic system consisting of 1800 water molecules was built initially, followed by an energy minimization for 10000 steps to remove atom overlapping, MD simulation with *NVT* ensemble for 2.0 ns for faster equilibration, and MD simulation with *NPT* ensemble run for 20.0

ns. The density of water predicted agrees with the experimental value of 1.0 g/cm^3 at 20.0 °C [30]. The equilibrated water unit cell was replicated to build a larger water system consisting of 32043 molecules. The final dimension of the system was 100.0 Å ×100.0 Å ×100.0 Å, which was used for the large interface systems. MD simulation with *NPT* ensemble was performed for another 30.0 ns for final equilibration.

Pure Heptane A cubic system consisting of 150 heptane molecules was built initially. Energy minimization was performed for 10000 steps followed by equilibration for 2.0 ns and *NPT* ensemble run for 30.0 ns. The predicted density of heptane was 0.66 g/cm^3, which is close to the experimental value of 0.68 g/cm^3 at 20.0 °C [30]. The equilibrated cubic heptane was replicated to build a larger heptane system consisting of 4212 molecules. The dimension of the system was 100.0 Å ×100.0 Å ×100.0 Å, which was used for the large interface system.

Air/Water Interface An air/water interface system was built. A water layer (consisting of 1924 molecules) adjacent to two vacuum layers having a height about 2.5 times as the water layer was built initially, and the dimension of the system was 35.0 Å × 40.0 Å × 300.0 Å. Energy was minimized for 10,000 steps and then equilibrated with *NVT* ensemble for 0.4 ns with a time step of 1.0 fs, followed by MD simulation with *NVT* ensemble for 20.0 ns with a time step of 2.0 fs.

Heptane/Water Interface A heptane/water interface system was built. Two equilibrated heptane layers (consisting of 600 molecules) were appended on the top and bottom of the water layer (with 1968 molecules) to build the heptane-water interface (**Figure 2a**) initially, and the dimension of the system was 35.0 Å × 41.0 Å × 140.0 Å. The thicknesses of the water and heptane layers were 40.0 Å and 50.0 Å, respectively. Energy was minimized for 10,000 steps and then equilibrated with *NVT* ensemble for 0.05 ns with a time step of 1.0 fs, followed by another equilibration with *NPT* ensemble for 0.6 ns with a time step 2.0 fs. Eventually MD simulation with *NPT* ensemble with a time step of 2.0 fs was run for 50.0 ns at 20.0 °C. An extension run of another 20.0 ns with *NVT* ensemble was performed for each system in order to calculate the interfacial tension.

3.2 Air/surfactant-monolayer/water Interface

The MD simulations of air/surfactant-monolayer/water interface structure shown in **Figure 2b** were performed with *NVT* ensemble using an orthorhombic box ($\alpha=\beta=\gamma=90.0°$, $L_x \neq L_y \neq L_z$) with a hexagonal close packing as initial conditions. The initial set up was generated from a fixed number of surfactant molecules, N_s=36 (6 by 6 array), area per surfactant molecule, A, total height of the system or box simulated, L_z=300, and an initial water layer thickness, L_{wi}, which changes as the simulation progresses. L_{wi} was specified as 40.0 Å for SDS, CTAB, and PFOA, and 60.0 Å for L77. The L_{wi} values were estimated based on the length of the hydrophilic group of molecules. The width of the box was obtained by $L_x = \sqrt{\frac{\sqrt{3}}{2} N_s * A}$ and $L_y = \frac{2}{\sqrt{3}} L_x$. The length of a single surfactant molecule in a vacuum (L_s) were calculated as 19.3 Å for SDS, 25.6 Å for CTAB,11.3 Å for PFOA, and 38.0 Å for L77. We then built the surfactant monolayer with the parameter values shown in **Table 1**. Finally, we appended the surfactant monolayer, water layer, and air together. We appended the layers in such a way that the head and tail groups of surfactants overlapped with the water and air layers respectively. For each run, we started with 10000 steps of minimization,

and then equilibrated the system with *NVT* ensemble for 0.4 ns with a time step of 1.0 fs. Eventually, we ran MD simulation with *NVT* ensemble for 20.0 ns with a time step of 2.0 fs.

For each surfactant, eleven MD simulations were performed with A varied as a parameter around the experimental value with a step size of 2.0~5.0 Å^2 as shown in **Table 1.** The experimental values of A at saturation of the interface were derived from the measured critical micelle concentration (CMC[9], [31-34]) in the bulk solution as explained later. For the surfactants without available experimental surface areas, we estimated A, based on the structure of the surfactant.

Table 1. Initial system setup for the MD-*NVT* simulations of air/surfactant-monolayer/water to calculate surface area, surface tension, and Gibbs elasticity calculation. N_w is the number of water molecules in the system.

SDS			CTAB			PFOA			L77		
T=27.0°C			T=25.0°C			T=30.0°C			T=25.0°C		
L_{wi} =40.0Å			L_{wi} =40.0Å			L_{wi} =40.0Å			L_{wi} =60.0Å		
A (Å^2)	L_x (Å)	N_w	A (Å^2)	L_x (Å)	N_w	A (Å^2)	L_x (Å)	N_w	A (Å^2)	L_x (Å)	N_w
33.0	32.1	1623	38.0	34.4	1877	34.0	32.6	1521	55.0	41.4	2261
36.0	33.5	1764	40.0	35.3	1968	37.0	34.0	1672	60.0	43.3	2490
39.0	34.9	1924	42.0	36.2	2055	40.0	35.3	1819	65.0	45.0	2728
42.0	36.2	2055	44.0	37.0	2149	43.0	36.6	1948	70.0	46.7	2953
45.0	37.5	2195	46.0	37.9	2253	46.0	37.9	2076	75.0	48.4	3186
48.0	38.7	2346	48.0	38.7	2346	49.0	39.1	2216	80.0	49.9	3427
51.0	39.9	2494	50.0	39.5	2439	52.0	40.3	2351	85.0	51.5	3668
54.0	41.0	2648	52.0	40.3	2542	55.0	41.4	2490	90.0	53.0	3904
57.0	42.2	2797	54.0	41.0	2648	58.0	42.5	2630			
60.0	43.3	2926	56.0	41.8	2742						
63.0	44.3	3066	58.0	42.5	2845						

MD simulations to calculate zeta potentials were performed for only one specified value of A for each of the three ionic surfactants (SDS, CTAB, and PFOA) as shown in **Table 2**. To study the dependence of Zeta potential on the initial water layer thickness L_{wi}, 6~8 MD simulations were performed with L_{wi} varied over the range of 40.0 to 90.0 Å with a step of 10.0 Å.

[9] CMC: critical micelle concentration

Table 2. Initial system setup for the air/surfactant-monolayer/water to run *NVT* simulations for zeta potential calculation. N_w is the number of water molecules in the system.

SDS		CTAB		PFOA	
T=27.0°C		T=25.0°C		T=30.0°C	
A=43.0Å^2 L_x=36.6Å		A=43.0Å^2 L_x=36.6Å		A=37.0Å^2 L_x=34.0Å	
L_{wi} (Å)	N_w	L_{wi} (Å)	N_w	L_{wi} (Å)	N_w
30.0	1448	40.0	1948	20.0	821
40.0	1948	50.0	2448	30.0	1241
50.0	2448	60.0	2932	40.0	1672
60.0	2932	70.0	3441	50.0	2098
70.0	3441	80.0	3944	60.0	2522
80.0	3944	90.0	4451	70.0	2954
90.0	4451			80.0	3387
				90.0	3830

3.3 Heptane/surfactant-monolayer/water Interface

MD simulations were performed on the heptane/surfactant-monolayer/water interface (**Figure 2c**) with *NPT* ensemble using an initial setup similar to the air-water system with 36 surfactant molecules. The initial values of the area per surfactant molecule A_i are given in **Table 3**. The area per molecule will change with time and reach a steady-state value for A at the end of simulation. We then took the water and heptane layer from the large pure systems with the same dimensions as the surfactant monolayer (L_x and L_y). We appended the water and heptane layers in such a way that the head and tail groups of the surfactants overlapped with the water and heptane layers respectively. The thickness of the water and heptane layers were selected so that the tail end of the surfactant monolayers did not interact with each other. The thickness and number of molecules for water and heptane are shown in **Table 3**. The total thickness L_{Zi} is the summation of the initial water layer thickness L_{wi} and the initial heptane thickness L_{hi}, $Lz_i = Lw_i + 2Lh_i$ which is 140.0 Å. The details of the simulation systems built are shown in **Table 3**. For each run, we started with 10000 steps of energy minimization, and then equilibrated with *NVT* ensemble for 0.05 ns with a time step of 1.0 fs, followed by another equilibration with *NPT* ensemble for 0.6 ns with a time step 2.0 fs. Eventually, we ran MD simulations with *NPT* ensemble for 50.0 ns with a time step of 2.0 fs. We also performed the extension run for another 20.0 ns with *NVT* ensemble in order to calculate the interfacial tension.

Table 3. Initial system setup for the heptane/surfactant-monolayer/water (*NPT*) simulations. N_w and N_h are the number of water and heptane molecules in the system, respectively.

Surfactants	T (°C)	Lw_i (Å)	Lh_i (Å)	Lz_i (Å)	A_i (Å^2)	Lx_i (Å)	N_w	N_h
SDS	27.0	40.0	50.0	140.0	40.0	35.3	1968	600
					50.0	39.5	2439	740
CTAB	25.0	40.0	50.0	140.0	40.0	35.3	1968	600
					50.0	39.5	2439	740
PFOA	30.0	40.0	50.0	140.0	35.0	33.0	1723	524
					40.0	35.3	1968	600
L77	25.0	60.0	40.0	140.0	60.0	43.2	4373	730
					70.0	46.7	5113	850

3.4 Experimental measurement of Surface and Interfacial Tensions

The static surface and interfacial tensions were measured using a tensiometer with a Du Noüy ring [31] (Sigma 701 Tensionmeter, Biolin Scientific, Linthicum Heights, MD) for all four surfactants. In this method, force exerted at the air/water and n-heptane/water interfaces is measured by submerging a metal ring through the interface. SDS was procured from Sigma-Aldrich Co. (St. Louis, MO, CAS 151-21-3, ≥99.0% purity) CTAB was from Kodak Inc. (Rochester, NY, Cat. 1179548), PFOA was from Acros Organics Inc. (Belgium, 96.0% purity, CAS 335-67-1), and Silwet-L77 was from Momentive Inc. (Round Rock, TX, Cat. No. VIS-30). Surfactant solutions were prepared with distilled water at various concentrations. 3.5 mL of solution was used for surface tension measurements and 10.0 mL of solution was used for interfacial measurements. The ring was submerged through the air/liquid interface 10 times and averaged for the reported surface tension. For the liquid/liquid interfaces, the ring was submerged once and the force measured, the test was then repeated to average two values for the reported interfacial tension. Error between measurements for the surface and interfacial tensions were less than 0.5 dyn/cm. Measurements were collected at solution temperatures of 20.0°C.

4. RESULTS

The MD-based structural properties of interfaces were calculated and discussed in the following sections.

4.1 Interface without a surfactant

4.1.1 Surface and Interfacial Tension

The terms surface tension and interfacial tension refer to air-water and heptane-water interfaces respectively. The surface and interfacial tensions γ were calculated from pressure as shown in **equation (1)** [13],

$$\gamma = 0.5 \int_0^{L_z} [P_N(z) - P_T(z)]\, dz \quad , \qquad (1)$$

where P_N and P_T are the normal and tangential components of the stress and were obtained from MD simulations. L_Z is the length perpendicular to the interface. The factor of 0.5 is due to the presence of two interfaces in the simulation box. In the bulk phase, P_N and P_T are very close, so the bulk phase barely contributes to the interfacial tension.

In MD simulations, pressure was averaged over the computational domain in each direction using **equation (2)**. Surface tension was calculated using **equation (3)** [32].

$$P_{dd} = \rho k_B T + \frac{1}{V}\sum_{i=1}^{N-1}\sum_{j=i+1}^{N} r_{ij}^{d} f_{ij}^{d} \quad , \qquad (2)$$

$$\gamma = 0.5 L_z \left[\langle P_{zz}\rangle - 0.5\left(\langle P_{xx}\rangle + \langle P_{yy}\rangle\right)\right] \quad , \qquad (3)$$

where the subscript d represents dimension x, y or z, while r and f are distance and force respectively between the atomic pairs in each calculated dimension, and N is the total number of atoms. P_{dd} is ensemble averaged pressure, which is a function of time and it exhibits large fluctuation. In the case d=z, P_{zz} and its moving average with time $\langle P_{zz}\rangle$ predicted by MD simulations are shown in **Figure 3** for SDS. The value of $\langle P_{zz}\rangle$ at the end of simulation was used to calculate surface tension using **equation (3)**.

C36FF [10] is one of the most accurate all-atom force fields for the prediction of monolayer properties that are related to the surfactant packing, such as surface area and hydrophobic tail dynamics [33, 34]. However, C36FF was generated based on TIP3P water model [11, 12]. The surface tension of the air/water interface obtained from MD simulations based on TIP3P is 53.0 ± 0.4 dyn/cm instead of experimental value of 72.0 dyn/cm at 25.0 °C [35]. The surface tension is under predicted and is typical of predictions made for water by others using other water models, such as TIP4P, SPC, F3C, and Ferguson possibly due to limited simulation time to reach vapor-liquid equilibrium [36, 37]. Because our interest was to examine the effect of surfactant, we choose to use 72.0 dyn/cm as the baseline and made a correction to the MD-based surface tension of the air/water and air/surfactant-monolayer/water interfaces by adjusting the predicted surface tension by 19.0 dyn/cm higher in this paper. Similarly, the MD-based interfacial tension of the pure heptane/water interface is 44.3 ± 0.7 dyn/cm, which is 6.9 dyn/cm lower than the experimental value of 51.2 dyn/cm [38]. Therefore, MD prediction for the interfacial tension of the heptane/surfactant-monolayer/water interfaces was adjusted by 6.9 dyn/cm higher in this work.

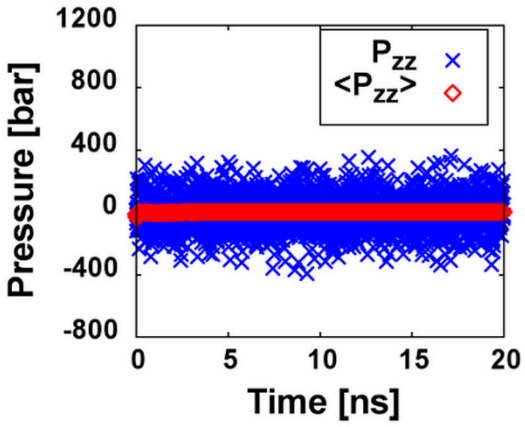

Fig. 3

Normal pressure P_{zz} and its moving average as functions of time predicted by MD simulations for air/SDS-monolayer/water system with *NVT* ensemble with surface area per molecule A=42.0 Å^2.

4.1.2 Component Density Profile and Interfacial Thickness

For the heterogeneous systems, atomic number density profile along the z-axis direction (normal to the surfactant monolayer) was calculated using MD simulation (*NPT*) and the mass density profile of each component was obtained ($\rho_j(z) = \sum_{i=1}^{N} n_{ij}(z) * m_i/N_A$, where n_i and m_i are atomic number density and mass of atom i of component j at z, N is the number of atoms in each component, and N_A is Avogadro's number). The density profiles of heptane/water are shown in **Figure 4,** which corresponds to the systems shown in **Figure 2a**.

Based on the component density profiles of the heptane/water interface, the interfacial thicknesses can be calculated. Since the interfaces are continuous in the MD simulations, the interfacial thicknesses were defined based on the "10-90" rule described in previous work [22, 39]. As shown in **Figure 2a** and **Figure 4a**, there are heptane bulk phases on the top and bottom of the box, water bulk phase in the center of the box, and heptane-water interfaces located between these bulk phases (near -25.0 Å and 25.0 Å). As shown in **Figure 4b**, the interfacial thickness of the heptane (d_h) is defined as the distance between the 10% and 90% of maximum heptane density. Similarly, the interfacial thickness of water (d_w) was calculated as the distance between 10% and 90% of the maximum water density. The total interfacial thickness (d_t) was defined as the distance between the position of 90% of the maximum density of heptane and water ("90-90") [13]. The d_t of the heptane-water interface without surfactants was calculated to be 4.1 Å at 20°C, which agrees well with the experimental value of 4.2 ± 0.2 Å [40] at 25°C. The good agreement between our MD predictions and experimental measurements demonstrates that C36FF with TIP3P water model results in accurate interfacial thickness values as well as component density profiles.

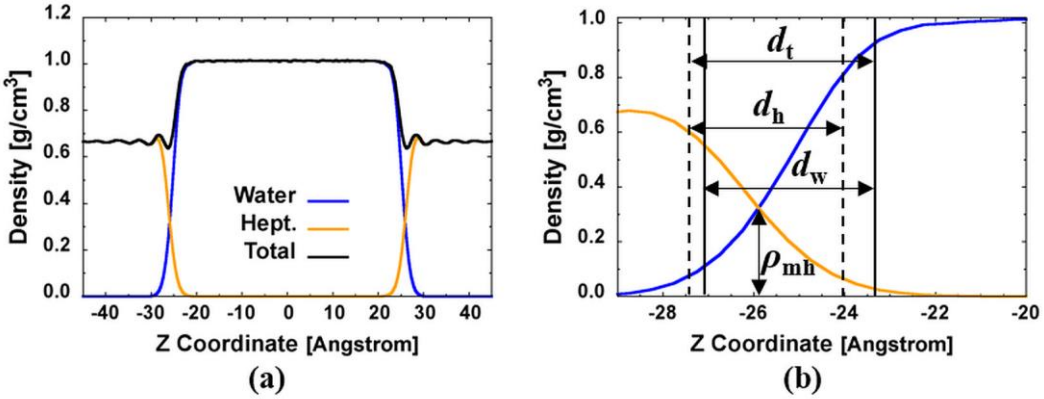

Fig. 4

(a) MD simulated component density profile of heptane/water interface without surfactant as function of z coordinate along the direction normal to the interface. (b) Zoom-in view of the interface region to show different interfacial thicknesses d_i. ρ_{mh} is the density of equal parts heptane and water within the interface.

4.2 Air/Surfactant-monolayer/Water Interface

When surfactants were introduced to the air/water interface, they interacted with water and changed the properties of the interface as discussed next.

4.2.1 Surface Area and Surface Tension Relation

The most probable surface area per molecule in the air/surfactant-monolayer/water interface A_m is an important property obtained from MD simulations, because it affects other interfacial properties. In literature, A_m was obtained by fitting the measured surface pressure and measured bulk density to the Szyszkowski equation for PFOA [41]. Moreover, A_m of SDS was directly measured by neutron reflectivity [42]. There are also other experimental methods such as small–angle neutron scattering (SANS) [43] or X-Ray reflectivity [44] for measuring A_m. We calculated A_m by combining surface tension measurements with the Gibbs equation as explained below.

Surface tension of the water-air interface decreases with increased concentration of surfactant at the interface until the saturation point is reached. The decrease in surface tension with increased surfactant concentration at the interface was predicted by MD simulations (*NVT*) by varying the specified value of *A* as a parameter as shown in **Table 1.** In practice, it is hard to measure the surfactant density at the interface directly, making it difficult to validate the MD predictions. However, the surface tension can be easily measured as a function of concentration of surfactant in the bulk solution. We fit the experimental data to a polynomial first and calculated the slope, which was used in the Gibbs equation to obtain the area per surfactant molecule at the interface. A recent study showed that the surface area at CMC obtained by Gibbs equation is within 1 Å^2 from the measurements by neutron reflection [45]. Below, we present the experimental data for surface tension and its relationship to area per molecule derived from the data followed by comparison with MD predictions.

Before the interface is saturated with surfactant, Gibbs equation [46] relates surface tension and bulk density of surfactant to the density of the surfactant at the interface by **equations (4)** and **(5)**,

$$C_s = -\frac{d\gamma/d(lnC_b)}{RT} \quad , \tag{4}$$

$$A = \frac{1}{N_A C_s} \quad , \tag{5}$$

where C_s is surface density of surfactant in mole/m^2, C_b is bulk density of surfactant in mole/m^3, γ is surface tension, R is gas constant, T is temperature, N_A is Avogadro's number, and A is the cross-sectional surface area per molecule.

Figure 5a-d show our measurements of surface tension as a function of natural logarithm of bulk density ln(C_b). The figures show that as the concentration of surfactant in the bulk is increased, the surface tension decreases and reaches a constant value at saturation. After the surfactant concentration reaches saturation, a further increase has little effect on the surface tension. In the literature, both first- and second-order polynomial fittings methods were used to calculate the slope in **equation (4)** from experimental data [46]. We fit the data with a (downward) second order polynomial function

$$\gamma = a[ln(Cb) + b]^2 + 72.0 \quad , \tag{6}$$

where C_b is bulk density of surfactant in mole/m^3, γ is surface tension, a and b are the parameters obtained from fitting. **Equation (6)** meets the requirements that the C_s is positive and C_s increases as $ln(C_b)$ increases before saturation. The polynomial fit to the experimental data was used to evaluate the numerator on the right hand side of **equation (4)**, which was used to calculate the concentration of surfactant at the interface. Then the surface area per molecule at each bulk density was calculated using **equation (5)**.

For MD simulations, **equations (1)-(3)** predict changes in pressure and surface tension with surface area per molecule at the interface, *A*, for different surfactants. The computations were unable to predict the asymptotic behavior after the interface gets saturated with surfactant. This is possibly because MD can only be run for a short period of time (in nanoseconds time scale), during which the excess surfactant cannot quickly migrate from the interface to the bulk. **Figure 5e-h** show a comparison of MD predictions with the experimental data using Gibbs-equation (GE_2). The results show good agreement between MD and GE_2 for the hydrocarbon and fluorocarbon surfactants SDS (**Figure 5e**) and PFOA (**Figure 5g**) respectively. **Figure 5e-h** also show good agreement between MD predictions and direct experimental measurements (labeled EXP) of surface area per molecule at saturation and surface tension reported in the literature [41, 42, 47-50]. However, there are quantitative differences between MD predictions and GE_2 for the hydrocarbon and trisiloxane surfactants CTAB and L77 (**Figure 5f and 5g** respectively) possibly due to high sensitivity to the calculation of slope using a polynomial fit of the experimental data.

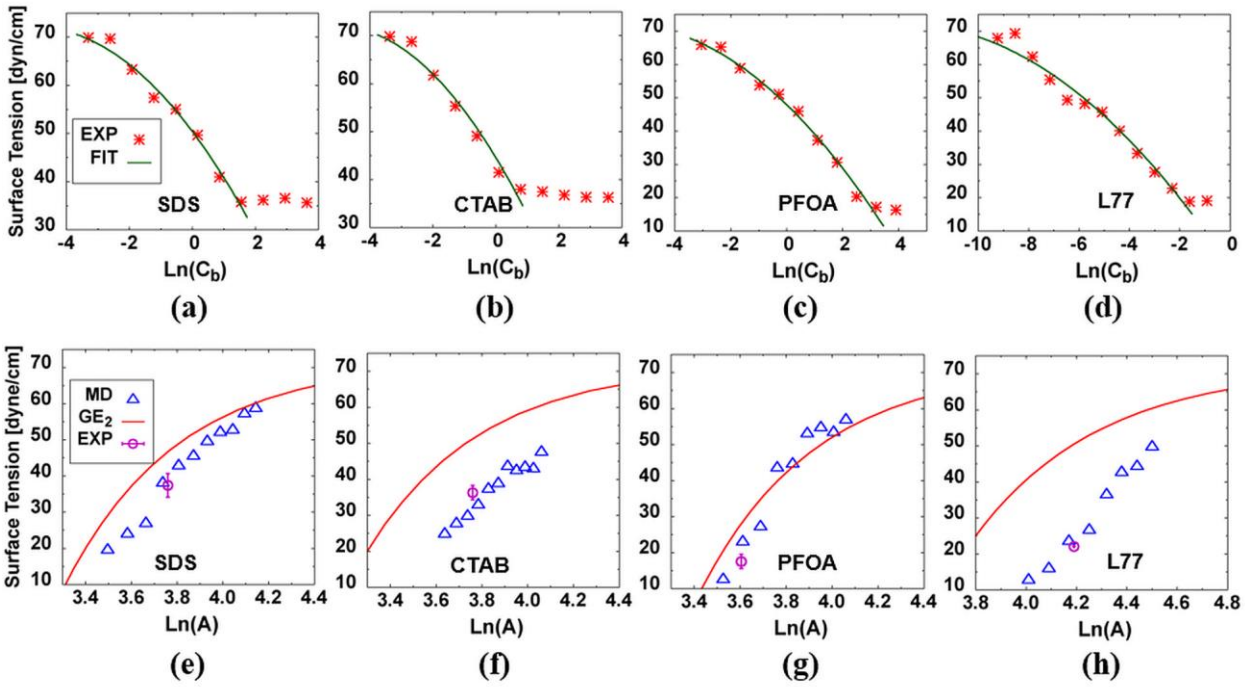

Fig. 5

(a)-(d) Experimental measurements of surface tension versus concentration (mole/m^3) of surfactant in the bulk solution and 2nd order polynomial fit to the experimental data to calculate area per molecule *A* using Gibbs-equation. The uncertainty for each experimental surface tension measurement is 0.5 dyn/cm. (e)-(h) Comparison of surface tension versus surface area per molecule calculated from Gibbs equation (GE_2) with MD-predictions. The purple data indicate the direct measurement of surface area per molecule and surface tension at saturation for SDS [42,

47], CTAB [48], PFOA [41, 49], and L77 [50]. For consistency, all MD predicted surface tension values including that of pure water are adjusted by 19.0 dyn/cm higher to correct for the TIP3P water model.

4.2.2 Gibbs Elasticity (E) and Most Probable Surface Area per Molecule (A_m)

The Gibbs elasticity E of a film describes the strength of the intermolecular interactions between surfactant molecules at an interface. It is an indication of the capability of a monolayer to resist change in surfactant packing or area per molecule due to stretching of the interface, which is a measure of the film stability. E is given by

$$E = d\gamma/d(lnA)\ , \qquad (7)$$

where γ is the surface tension and A is the surface area per molecule of surfactant. E can be determined from MD simulations, which are shown in **Figure 6**. **Figure 6a** shows the MD predictions for surface tensions of different surfactants that were already shown in **Figure 5e-h**. **Figure 6a** also shows a third order polynomial (with the negative coefficient of the highest order) fitted to the MD predictions of surface tension by

$$y = -|a|x^3 + bx^2 + cx + d \quad , \qquad (8)$$

where x is the natural logarithm of surface area per molecule A, y is the surface tension, and a, b, and c are the parameters obtained from fitting.

The trisiloxane has large A values because of its branched tail as one may expect. The surface tension curve is very steep for PFOA among the surfactants studied. As the logarithm of surface area increases, the surface tension increases, trending in an "S" shape. Then by taking the derivative of the fitted polynomial, E was obtained as a function of $ln(A)$ as shown in **Figure 6b**. **Figure 6b** shows downward opening parabolas with maxima for different surfactants. The A value corresponding to the maximum Gibbs elasticity (E_m) is defined as the most probable surface area per molecule A_m. The maximum E indicates an interface's capacity to increase surface tension in response to imposed surface dilatation, therefore at this point the surfactant is most stable and resists surface dilatation or surfactant concentration fluctuations by retaining a uniform packing. The E_m and A_m values obtained from **Figure 6b** are shown in **Figure 6c**. **Figure 6c** shows that the E_m value predicted by MD simulation for CTAB monolayer was 64.6 dyn/cm at 25.0 °C, and agrees well with experimental value of 61.0 dyn/cm measured at 23.0 °C [48]. Experimental measurements of E_m for the other three surfactants were not available to our knowledge. The MD simulations show that the fluorocarbon surfactant PFOA has the greatest E_m (119.4 dyn/cm) and thus it is most stable, the siloxane surfactant L77 has an intermediate E_m value (90.9 dyn/cm), while hydrocarbons SDS (75.5 dyn/cm) and CTAB have the lowest values of E_m among the four surfactants. A surfactant is adsorbed on lamellae of bubbles within the foam structure. In foam stability experiments, foams are generated from different surfactants and degradation rates of a foam layer are measured with time [3-5]. The order of the Gibbs elasticity values predicted by MD for different surfactant monolayers are qualitatively consistent with the foam stability measurements for SDS, perfluorocarbon surfactants and hydrocarbon surfactants [3-5].

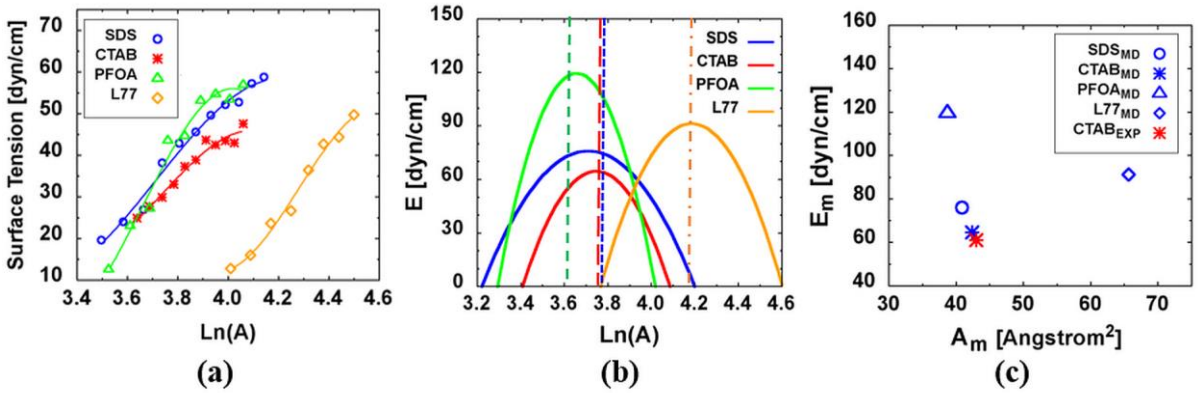

Fig. 6

(a) The MD predictions for surface tension as functions of surface area per molecule, A, along with 3rd order polynomial fits (solid lines) for calculating maximum Gibbs elasticity, E_m. The uncertainty for each experimental surface tension measurement is 0.5 dyn/cm. (b) The MD-predicted Gibbs elasticity as functions of $ln(A)$. The vertical lines indicate the experimental values for surface area per molecule [41, 42, 48, 50]. (c) The most probable surface area at maximum Gibbs elasticity of surfactant monolayer obtained from MD simulations compared with experimental values of E_m and A_m for CTAB surfactant monolayer [48].

4.2.3 Comparison of MD-based A_m and γ_m with Experiments

The MD predictions of A_m were compared with experimental data [41-44, 48, 50] and the MD simulation results of Jang et al. [13] in **Figure 7a**. The results show that the A_m obtained from simulations agree reasonably well with experiments, with deviations less than 3.0 Å^2 for all four surfactants. The area of siloxane surfactant L77 is significantly larger than both the hydrocarbons, SDS and CTAB, and the fluorocarbon PFOA due to the long oxyethylene chain in the head group and also the bulky tri-siloxane group in the tail. PFOA has the smallest area due to its small head group (**Figure 1**). Zhuang et al. [34] showed that with the same tail, the surface area increases as the size of the head group increases; with the same head group, the surface area decreases as the hydrocarbon chain length increases due to stronger hydrophobic interaction of the tails. Therefore, the surface areas of SDS and CTAB are close because CTAB has a larger head group (trimethylamine) and longer hydrocarbon tail than SDS.

Figure 7b shows that the surface tension at saturation (γ_m) corresponds to E_m and A_m in **Figure 6c**. Small differences in the most stable surface area per molecule A_m can lead to rather large differences in the surface tension especially for PFOA which has the steepest curve as shown in **Figure 6a.** For PFOA, the predicted surface tension is noticeably higher than experimental values (**Figure 7b**). Nevertheless, the good agreement between the MD predictions for A_m and γ_m with the experimental data shows that our method based on the maximum in E_m for determining A_m and γ_m works well for the surfactants studied in this work. The A_m values from our calculations of the air-water interface using C36FF agree well with previous calculations of Newton black films by Jang and Goddard [13] for SDS and CTAB using DREIDING force-field as shown by blue bars in **Figure 7a**. Rusanov et al. [51] developed a thermodynamic model for thin and thick films relating Gibbs elasticity and disjoining pressure. The model predicts a peak in elasticity as the surfactant concentration approaches CMC. Their model predictions suggest that E_m corresponds

to CMC consistent with the comparisons shown in **Figure 7b**. The A_m we defined represents the most stable packing, and requires the highest energy and force and it corresponds to E_m.

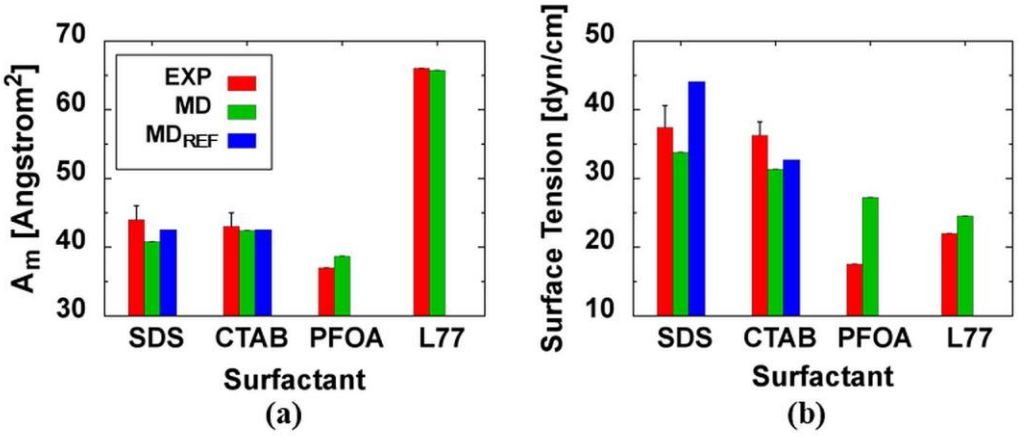

Fig. 7

(a) The comparison of MD predicted (MD) most stable surface area per molecule A_m with the experimental data (EXP) for SDS [42], CTAB [48], PFOA [41], and L77 [50], and MD simulation results reported in the literature [13] (MD_{REF}). (b) Comparison of the MD predicted surface tensions at saturation γ_m with the experimental data for SDS [47], CTAB [48], PFOA [49], and L77 [50], and MD simulation results in literature [13].

4.2.4 Zeta potential (ζ)

From the MD simulations, the atomic number density profile of atoms involved in the charged groups was calculated. The density profile of a charged group (e.g. SO_4^{2-} in SDS) is the summation of the atomic number density profile normalized by the atomic partial charge. We can then obtain the net charge density profile of the air/surfactant-monolayer/water interface for ionic surfactants by adding up the density profiles of the charged groups. **Figure 8** shows four times the net charge density (Net×4). As shown in **Figure 8**, the charge density profile of CTAB shows the broadest charge distribution, and the smallest peak, while PFOA shows the narrowest charge distribution with the greatest peak. The outer Helmholtz plane (OHP) is defined as the plane at which the net charge density starts to decrease as we progress from the bulk water region (z=0.0) to the surface [52]. The location of the OHP for the three surfactant interfaces are indicated by the black vertical lines in **Figure 8**. It was found that the electrostatic potential at the OHP is equivalent to the zeta potential [53], which is related to the stability of the air/surfactant-monolayer/water film. The maxima in net charge density are the highest for PFOA followed by SDS and CTAB, which is in the reverse order of head group size.

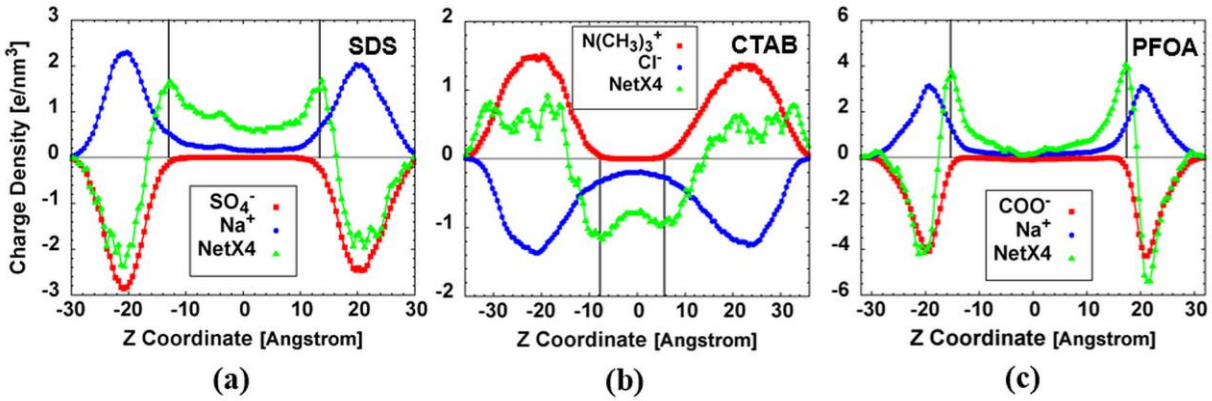

Fig. 8

The MD-based charge density profile of charged groups in SDS, CTAB, and PFOA, the counter ions, and the net charge when the initial water layer thickness is 50.0 Å. The black vertical lines indicate the locations of the OHP.

To calculate the electrostatic potential, we used the method described in [52]. Only the explicit free charges, such as the surfactant charge group and the counter ions, were used to calculate the potential, while the effects of water and air were included in the local dielectric constant. Therefore, the electrostatic potential of nonionic L77 could not be calculated. The local dielectric constant, ε (z), (consider the solvent phase only) was calculated by the Clausius−Mossotti relation [54].

$$\frac{\varepsilon(z)-1}{\varepsilon(z)+2} = \left(\frac{\rho_1(z)}{\rho_{1,0}}\right)\left(\frac{\varepsilon_{1,0}-1}{\varepsilon_{1,0}+2}\right) + \left(1-\frac{\rho_1(z)}{\rho_{1,0}}\right)\left(\frac{\varepsilon_{2,0}-1}{\varepsilon_{2,0}+2}\right) = K(z) \qquad (9)$$

$$\varepsilon(z) = \frac{1+2K(z)}{1-K(z)} \qquad (10)$$

Where ε(z) is local dielectric constant at z, $\rho_1(z)$ is the density of the water atoms at z, and $\rho_{1,0}$ is the corresponding pure (bulk) water phase limit. $\varepsilon_{1,0}$ and $\varepsilon_{2,0}$ are the dielectric constants of pure water (80.1) and air (1.0) respectively.

The Poisson's equation based on Coulomb's law and Gauss's theorem is given by **equation (11)**.

$$\nabla \cdot \varepsilon\epsilon_0 E_f = -\nabla \cdot \varepsilon\epsilon_0 \nabla V = -\nabla \cdot \varepsilon\epsilon_0 \nabla V = \rho_c \qquad (11)$$

Where ε is the local dielectric constant (i.e. relative permittivity), ϵ_0 is the vacuum permittivity (8.9×10^{-12} $C\cdot V^{-1}\cdot m^{-1}$), E_f is the electric field (not the Gibbs elasticity E), V is the electrostatic potential, and ρ_c is the net charge density profile.

Considering the z-dimension (along the direction normal to the monolayer surface) only, the net charge density profile $\rho_c(z)$ was fitted to a polynomial by assuming that the electric field and potential are zero at the center of bulk water phase. The MD-based electrostatic potential was calculated by integrating the Poisson equation given by **equation (11)** and dividing by the local electric constant at each z bin to calculate the electric field as shown in **equation (12)**. To carry out the integration, the electric field data was fitted to a polynomial function, which was integrated to obtain the electrostatic potential as shown in **equation (13)**.

$$E_f(z) = \frac{q_e}{\varepsilon(z)\epsilon_0} \int \rho_c(z) dz \quad (12)$$

$$V(z) = -\int E_f(z) dz \quad (13)$$

Where $\rho_c(z)$ is the net charge density at z, and q_e is charge of an electron (1.6 x 10^{-19} C).

The electrostatic potentials as functions of z with an initial water layer thickness of 50.0 Å for SDS, CTAB and PFOA are shown in **Figure 9**. CTAB has a positive potential due to a negative net charge at the OHP, while SDS and PFOA have negative potentials due to the positive net charge at the OHP (**Figure 8**). The potential is 0.0 V at the center of bulk water, and the magnitude of potential increases as the z approaches the edge of the air/monolayer/water interface. The potentials at the OHPs, i.e. the zeta potentials, of surfactant systems are also shown by the vertical lines in **Figure 9**.

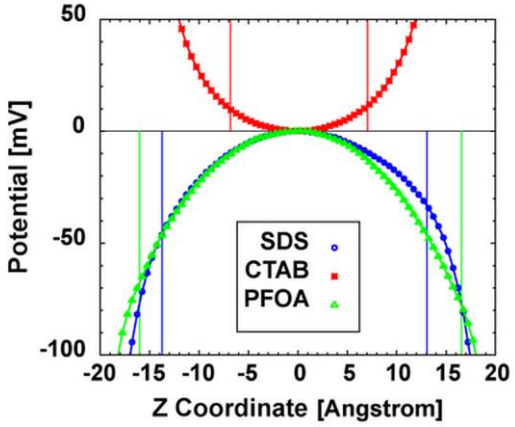

Fig. 9

The MD-based electrostatic potential of SDS, CTAB, and PFOA in the air/surfactant-monolayer/water interface with an initial water layer thickness of 50.0 Å. The vertical lines indicate the location of the OHP.

The dependence of the MD predicted zeta potential on the initial water layer thickness L_{wi} is shown in **Figure 10a**. The results show that for the same L_{wi}, PFOA has the greatest zeta potential, SDS has the intermediate, and CTAB has the smallest potential. Because the number of ions is fixed, as the L_{wi} increases, the zeta potential increases for all the three surfactants due to the reduced charge density of counter ions in the interface region as expected from previous work [55]. Both the maximum Gibbs elasticity E_m and the zeta potential characterize the stability of the surfactant monolayer. The E_m describes the capability of the monolayer to resist change in surfactant packing along the surface, while the zeta potential describes the capability of the monolayer to resist change in water film thickness, which is the change in the direction normal to the surface. Therefore, we would like to study the possible correlation between them. Pearson's correlation coefficient (r) is calculated to describe the linear association of two properties.

$$r = \sum_{i=1}^{M}(x_i - \bar{x})(y_i - \bar{y}) \Big/ \left(\sqrt{\sum_{i=1}^{M}(x_i - \bar{x})^2} \sqrt{\sum_{i=1}^{M}(y_i - \bar{y})^2} \right), \quad (14)$$

where M is the number of type of surfactant, which is four in this work. x_i and y_i are the two property values for surfactant i, and $\bar{x}$ and $\bar{y}$ are the mean of each property values, respectively.

Pearson's correlation coefficient (r) near 1.0 indicates positive linear correlation, and -1.0 for negative linear correlation, while 0.0 suggests no linear correlation. With the same initial water layer thickness L_{wi}, the maximum Gibbs elasticity E_m and the absolute value of the zeta potential have strong linear correlation with a coefficient of 0.95 (**Figure 10b**), which suggest possible positive and linear correlations of two types of stabilities.

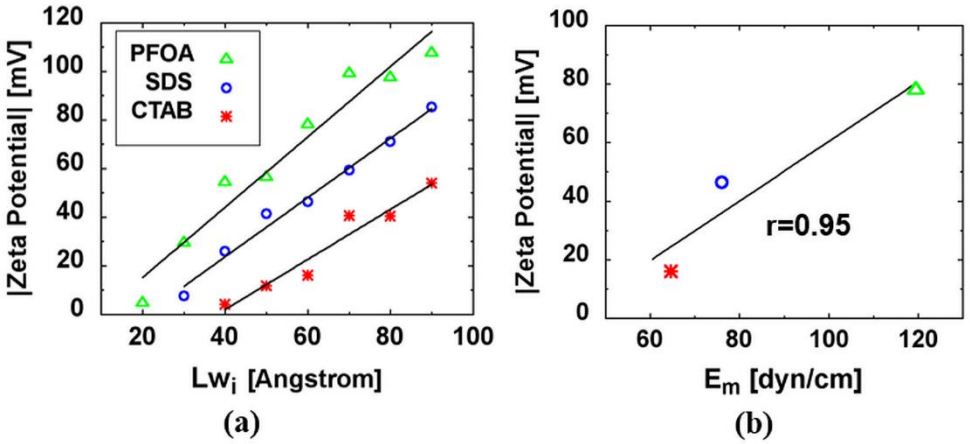

Fig. 10

(a) MD simulated magnitude of zeta potential as a function of the initial water layer thickness (b) The correlation between the maximum Gibbs elasticity E_m and the magnitude of the zeta potential, with an initial water layer thickness of 60.0 Å shown with the corresponding Pearson correlation coefficients.

4.3 Heptane/Surfactant-monolayer/Water Interface

4.3.1 Most probable surface area per molecule (A_{mh}) and Interfacial Tension

The most probable surface area per molecule of the heptane/surfactant-monolayer/water interface (A_{mh}) was calculated by

$$A_{mh} = L_x L_y / N_s \quad , \qquad (15)$$

where L_x and L_y are the box lengths in the x and y directions, respectively, and $L_x L_y$ is the MD-predicted total cross sectional area. N_s is the total number of surfactants per monolayer, which is specified as 36.

The MD simulations search the most thermodynamically stable state, i.e. the minimum energy state. For MD simulations are performed with *NPT* ensemble and with a given initial surface area per molecule (A_i). The monolayer changes its packing as the simulation progresses, and finally converges to the lowest energy packing that corresponds to the most probable (stable) surface area per molecule in the presence of heptane (A_{mh}). The surface area per molecule and its moving average as a function of simulation time for the heptane/surfactant-monolayer/water interface for the four surfactants are shown in **Figure 11.** The results show that the surface area converges to the same value (A_{mh}) regardless of the initial A_i, and all the surfactant monolayers reach equilibrium by 30.0 ns.

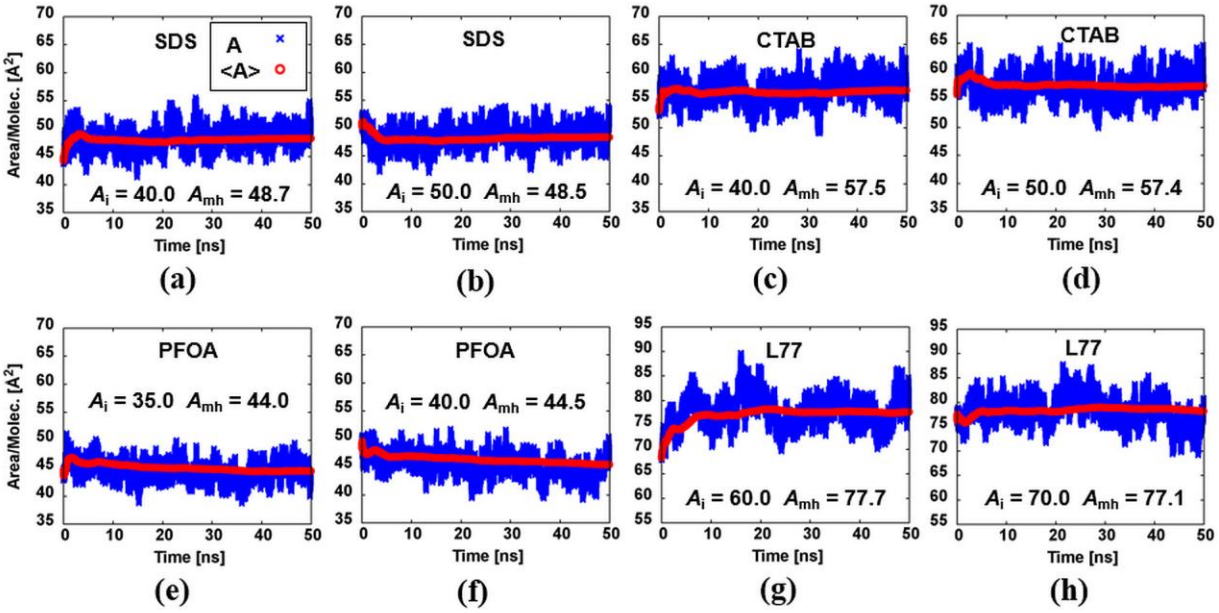

Fig. 11

The surface area per molecule and its moving average as a function of simulation time for the heptane/surfactant-monolayer/water interface simulations for different surfactants. The (A_i) (A_{mh}) values shown are the initial surface area per molecule and the final surface area per molecule after equilibrium respectively.

A comparison of the surface area per molecule of surfactant in the air/water and heptane/water interfaces is shown in **Table 4**. The results show that for the four surfactants studied, the presence of heptane increases the surface area of surfactants, i.e. $A_{mh} > A_m$. The surface area of CTAB shows the most significant increase and PFOA shows the smallest increase. The interfacial tension of the heptane/surfactant-monolayer/water interface was calculated using **equation (3)**. The interfacial tension was obtained from *NPT* initially followed by *NVT* simulation for 20.0 ns. The results are shown in **Table 4**. The interfacial tensions are dramatically lower than the surface tensions. The fluctuation (standard error of two runs) of the MD-predicted interfacial tension is greater than the differences among different surfactants. Therefore, the simulation has large uncertainty in predicting interfacial tension for different surfactants. **Table 4** compares MD predictions with our experimental measurements and measurements of interfacial tensions reported in the literature [56-58]. The experimental values also have large variations.

Table 4. MD predicted surface area per surfactant and surface tension or interfacial tension values at saturation for air/surfactant-monolayer/water interface (A_m and γ_m) and heptane/surfactant-monolayer/water interface (A_{mh} and γ_{mh}) are shown (average and error of two runs with two initial surface areas). Without surfactant, MD-predicted interfacial tension for heptane/water is 44.3 ± 0.7 dyn/cm compared to experimental value of 51.2 dyn/cm [38] at 20.0 °C. The MD calculated surface tensions and interfacial tensions are raised by 19.0 and 6.9 dyn/cm respectively to correct for TIP3P water model.

Systems	Air/Surfactant-monolayer/Water	Heptane/Surfactant-monolayer/Water

Properties	A_m	γ_m	A_{mh}	γ_{mh}	$\gamma_{mh,exp}$
	Å^2	dyn/cm	Å^2	dyn/cm	dyn/cm
SDS	40.8	33.8	48.6 ± 0.1	10.1 ± 1.9	6.1 ± 0.5, 7.5 [56][a], 11 [57][b]
CTAB	42.4	31.3	57.4 ± 0.03	7.3 ± 2.2	4.3 ± 0.5, 10.0 [57][b], 13.0 [58][c]
PFOA	38.7	27.2	44.3 ± 0.2	9.8 ± 2.8	9.9 ± 0.5
L77	65.7	24.5	77.4 ± 0.2	8.6 ± 0.9	4.7 ± 0.5

[a,b,c] Values reported are measured at [a] 22.0 °C, [b] 23.0 °C, [c] 25.0 °C.

4.3.2 Interfacial Thickness and Density of Heptane

The component density profile obtained from the heptane/surfactant-monolayer/water simulations are shown in **Figure 12**. The density profile for L77 corresponds to the interface system shown in **Figure 2c**. The component density profile describes the averaged location of each component, which can be used to calculate monolayer structural properties, such as the interfacial thicknesses and the density of heptane in the heptane and water mixture region (**Figure 4b**).

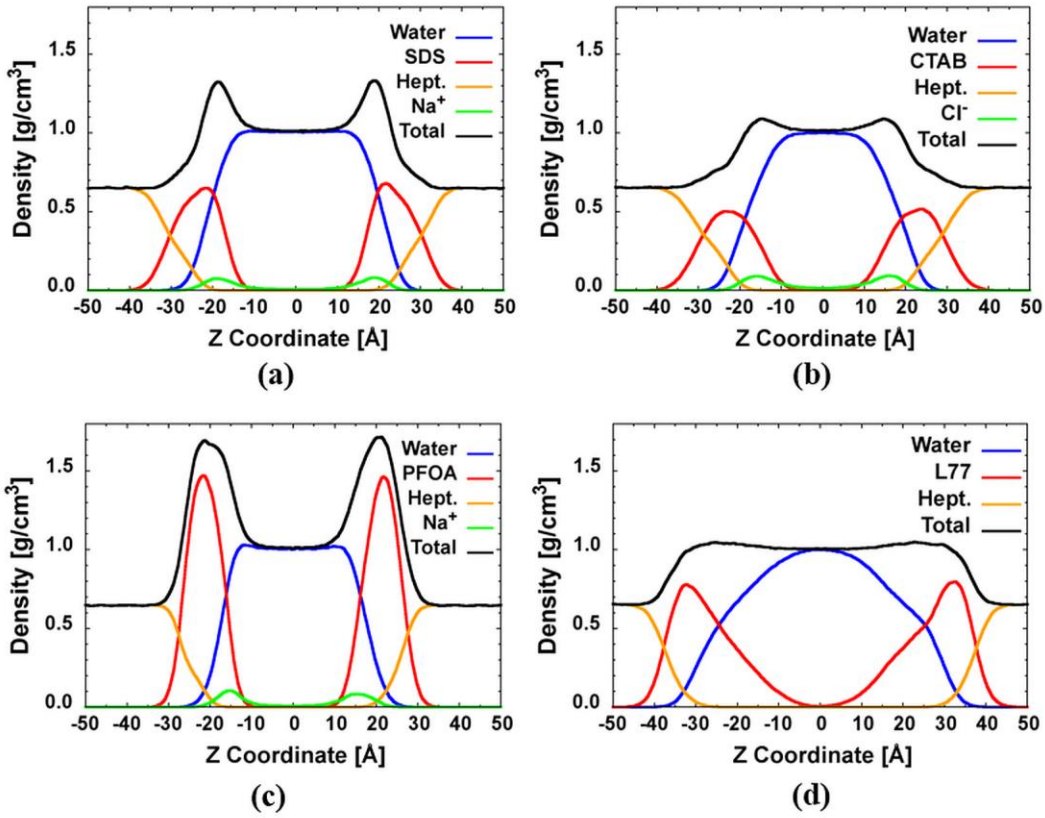

Fig. 12

MD simulated component density profile as a function of *z* coordinate along the direction normal to the interface for (a) heptane/SDS-monolayer/water system (b) heptane/CTAB-monolayer/water system (c) heptane/PFOA-monolayer/water system and (d) heptane/L77-monolayer/water system.

The "10-90" interfacial thickness of water (d_w) and heptane (d_h) for the heptane/surfactant-monolayer/water were defined in **section 3.1.2.** d_w and d_h represent penetration of water and heptane in the interface respectively and can be obtained from the density profiles shown in **Figure 12**. Similarly, interface thickness (d_s) is defined as the distance between locations where the surfactant density is 10% of the maximum density profile shown in **Figure 12**. A comparison of d_w for all systems is shown in **Table 5**, including systems with and without surfactants. The presence of heptane instead of air at the interface reduces the interfacial thickness of water d_w. **Table 5** also shows the interface thickness, d_s, is highest for L77 possibly due to the large trisiloxane tail and smallest for PFOA. Water penetrates the interface less for SDS (43.3%), CTAB (46.2%), and PFOA (45.5%) compared to L77 (68.1%) possibly because of the trisiloxane's long oxyethylene head. The degree of water penetration of the interface may be important to suppress the rate of heptane fuel transport across the interface.

A comparison of the MD calculated values of d_w and d_h for each surfactant is shown in **Figure 13a**. As we expect, both the d_h and d_w increase due to the presence of surfactants compared those in the absence of surfactants represented by (W-H) in **Figure 13a**. The MD-predicted A_{mh} and d_w (**Figure 13b**) show the same trend as the size of the polar head group of the surfactants which can be seen in **Figure 1**, i.e., A_{mh} and d_w increase as the size of the polar head group increases. L77 has the highest A_{mh} and d_w among the four surfactants, CTAB and SDS have intermediate values, and PFOA has the lowest ones. The value of d_w for L77 is much higher than those for other three surfactants. This may be due to its long hydrophilic head group. The value of d_h for L77 is almost as low as PFOA, which may be due to their oleophobic tails compared to the hydrocarbon tails of SDS and CTAB. It is possible that d_w depends on length of the polar headgroup, while d_h depends on the length or size of the hydrophobic tail. As shown in **Figure 13b**, the Pearson's correlation coefficient of 0.99 suggest the strong positive linear correlation between MD-based most stable surface area per molecule in the heptane/surfactant-monolayer/water A_{mh} and d_w, which indicates that the larger the area, the deeper the water can penetrate into the hydrophilic region based on the surfactants studied. However, the A_{mh} and d_h are not strongly correlated, which suggest that A_{mh} affects d_w more strongly than d_h for these surfactants. Water and heptane co-exist within the interface. The penetration distance of heptane into the interface is correlated with the density of an equal mixture of water and heptane ρ_{mh} (**Figure 13c**).

Table 5. Comparison of interfacial thickness of water d_w (Å), total interfacial thickness d_t (Å**),** and interfacial thickness of surfactant monolayer d_s (Å**) (**the distance between the positions of the 10% maximum surfactant density) for all systems

Without surfactant	Air/water (d_w)	Heptane/water (d_w)	Heptane/water Interface thickness (d_t)
	4.1 ± 0.03	3.7 ± 0.01	4.1 ± 0.01
With surfactant	Air/surfactant-monolayer/water (d_w)	Heptane/surfactant-monolayer/water (d_w)	Heptane/surfactant-monolayer/water (d_s)
SDS	11.6 ± 0.2	9.4 ± 0.1	21.7 ± 0.1
CTAB	19.9 ± 0.3	11.9 ± 0.2	25.8 ± 0.1
PFOA	8.4 ± 0.1	7.6 ± 0.1	16.7 ± 0.3
L77	23.9 ± 0.1	21.8 ± 0.7	32.0 ± 0.1

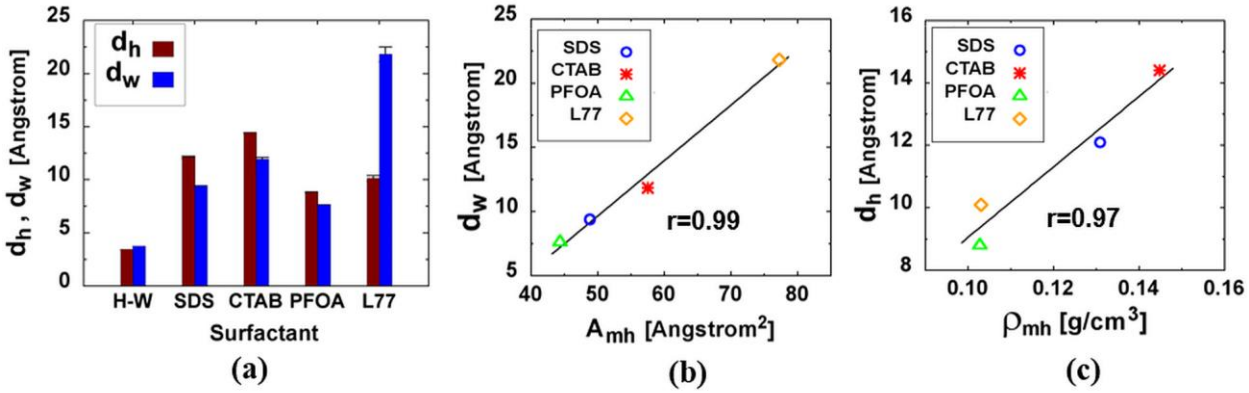

Fig. 13

(a) The comparison of the heptane and water interfacial thicknesses without and with surfactants. (b) The correlation between MD-based A_{mh} and d_w shown with a linear fit and the Pearson's correlation coefficient. (c) The correlation of the MD-based interfacial thickness of heptane and the density of heptane in the heptane/water mixing region.

5. CONCLUSIONS

Surfactants adsorbed at bubble lamellae can influence bubble stability and fluorosurfactants impose greater bubble stability in foams compared to hydrocarbon surfactants [3-5]. Some of the effect stems from the inherent interactions among a surfactant, water, and heptane at an air-water interface and heptane-water interfaces and have been investigated using MD simulations. We perform MD simulations of monolayers of surfactants for two hydrocarbon surfactants (SDS and CTAB), a siloxane surfactant (L77), and a perfluorocarbon surfactant (PFOA) and predict interfacial structures and properties.

We calculated the area per surfactant molecule, A, from the experimental measurements of surface tension γ versus concentration of surfactant in the bulk solution (**Figure 5a-d**). We showed good agreement between the MD predicted relationship between γ and A with that from the experiments (**Figure 5e-h**). We also calculated the most probable surface area per surfactant molecule, A_m, as the surface area corresponds to the maximum Gibbs elasticity E_m through MD simulations (**Figure 6**). Our calculations of E_m, A_m, and γ_m for CTAB laden air-water interface agreed reasonably well with the experimental data (**Figure 6-7** and **Table 4**). They also agreed with previous MD simulation results [13] for SDS and CTAB (**Figure 7**). The γ_m and E_m values predicted for the siloxane L77 were closer to the fluorocarbon surfactant PFOA than the two hydrocarbon surfactants. PFOA and L77 had higher E_m values which suggest higher interfacial stability to mechanical perturbations of the interface requiring a larger change in energy than for SDS and CTAB. Both the maximum Gibbs elasticity of surfactant monolayer E_m and the zeta potential are used to describe the stability of the surfactant monolayer, and they are strongly correlated to each other. The zeta potential of fluorocarbon PFOA were greater than the hydrocarbon SDS and CTAB, which suggest stronger stability of PFOA (**Figure 10**).

For the case of the heptane/water system, heptane penetration distance and density of heptane depend on the surfactants and shows that PFOA has the smallest values followed by the siloxane surfactant (L77), and the hydrocarbon surfactants (SDS, and CTAB) as shown in Figure 13c. The relatively small values of interfacial tensions are predicted less accurately by MD compared to the air-water surface tensions. The simulation results show that heptane has a much stronger effect on the interfacial properties (surface area, interfacial tension, and interfacial thickness of water) of CTAB than PFOA (**Table 4**).

6. FUTURE WORK

MD is a useful tool to understand the effects of structure-performance relationship for improving foam stability and fire suppression. The validated simulation methods will enable investigation of systematic structural changes to the surfactant molecule to increase lamella stability. This will provide structural features of potential surfactants for synthesis and experimental investigations, and facilitate the development of the new effective fire-fighting aqueous foams.

7. ACKNOWLEDGEMENTS

We would like to thank the Strategic Environmental Research and Development Program (SERDP) of the U.S. Department of Defense (DoD) for supporting this work via grants WP2739 and WP18-1592. We also would like to thank the US Office of Naval Research for funding this work through the Naval Research Laboratory Base Program. We also would like to thank the DoD for providing High Performance Computational resources; the simulations were performed on Thunder and Lightning clusters of Air Force Research Laboratory (AFRL) DoD Supercomputing Resource Center. We also would like to specially thank Dr.Wei Shi from the U.S. Department of Energy for sharing the key force field parameters of siloxane.

8. PERSONNEL

Xiaohong Zhuang[1,2], Katherine M. Hinnant[2], and Ramagopal Ananth[2]
[1]American Society for Engineering Education Postdoctoral Associate
[2]Chemistry Division, U.S. Naval Research Laboratory, Washington, DC 20375, United States

9. REFERENCES

[1] C. Lau, K. Anitole, C. Hodes, D. Lai, A. Pfahles-Hutchens, J. Seed, Perfluoroalkyl acids: A review of monitoring and toxicological findings, Toxicological Sciences, 99 (2007) 366-394.
[2] J.M. Conder, R.A. Hoke, W. De Wolf, M.H. Russell, R.C. Buck, Are PFCAs bioaccumulative? A critical review and comparison with regulatory lipophilic compounds, Environmental Science & Technology, 42 (2008) 995-1003.
[3] K.M. Hinnant, M.W. Conroy, R. Ananth, Influence of fuel on foam degradation for fluorinated and fluorine-free foams, Colloids and Surfaces A, 522 (2017) 1-17.
[4] M.J. Kennedy, M.W. Conroy, J.A. Dougherty, N. Otto, B.A. Williams, R. Ananth, J.W. Fleming, Bubble coarsening dynamics in fluorinated and non-fluorinated firefighting foams, Colloids and Surfaces A, 470 (2015) 268-279.

[5] M.J. Kennedy, M.W. Conroy, J.W. Fleming, R. Ananth, Velocimetry of interstitial flow in freely draining foam, Colloids and Surfaces A, 540 (2018).
[6] N.M. Kovalchuk, A. Trybala, V. Starov, O. Matar, N. Ivanova, Fluoro- vs hydrocarbon surfactants: Why do they differ in wetting performance?, Advances in Colloid and Interface Science, 210 (2014) 65-71.
[7] A. Czajka, G. Hazell, J. Eastoe, Surfactants at the design limit, Langmuir, 31 (2015) 8205-8217.
[8] V.H. Dalvi, P.J. Rossky, Molecular origins of fluorocarbon hydrophobicity, Proceedings of the National Academy of Sciences of the United States of America, 107 (2010) 13603-13607.
[9] S. Sett, R.P. Sahu, D.D. Pelot, A.L. Yarin, Enhanced Foamability of Sodium Dodecyl Sulfate Surfactant Mixed with Superspreader Trisiloxane-(poly)ethoxylate, Langmuir, 30 (2014) 14765-14775.
[10] J.B. Klauda, R.M. Venable, J.A. Freites, J.W. O'Connor, C. Mondragon-Ramirez, I. Vorobyov, D.J. Tobias, A.D. MacKerell, R.W. Pastor, Update of the CHARMM all-atom additive force field for lipids: Validation on six lipid types., Journal of Physical Chemistry B, 114 (2010) 7830-7843.
[11] S.R. Durell, B.R. Brooks, A. Bennaim, Solvent-induced forces between two hydrophilic groups, J. Phys. Chem., 98 (1994) 2198-2202.
[12] W.L. Jorgensen, J. Chandrasekhar, J.D. Madura, R.W. Impey, M.L. Klein, Comparison of simple potential functions for simulating liquid water, J. Chem. Phys., 79 (1983) 926-935.
[13] S.S. Jang, W.A. Goddard, Structures and properties of newton black films characterized using molecular dynamics simulations, Journal of Physical Chemistry B, 110 (2006) 7992-8001.
[14] Z. Gamba, J. Hautman, J. Shelley, M. Klein, Molecular Dynamics Investigation of a Newton Black Film, Langmuir, 8 (1992) 3155-3160.
[15] M. Tarek, D.J. Tobias, M.L. Klein, Molecular dynamics simulation of tetradecyltrimethylammonium bromide monolayers at the air/water interface, J. Phys. Chem., 99 (1995) 1393-1402.
[16] J. Chanda, S. Bandyopadhyay, Molecular dynamics study of surfactant monolayers adsorbed at the oil/water and air/water interfaces, Journal of Physical Chemistry B, 110 (2006) 23482-23488.
[17] H. Watarai, Y. Onoe, Molecular dynamics simulation of interfacial adsorption of 2-hydroxy oxime at heptane/water interface, Solvent Extraction and Ion Exchange, 19 (2001) 155-166.
[18] L. Zhang, Z.P. Liu, T. Ren, P. Wu, J.W. Shen, W. Zhang, X.P. Wang, Understanding the structure of hydrophobic surfactants at the air/Water interface from molecular level, Langmuir, 30 (2014) 13815-13822.
[19] M. Stone, S. da Rocha, P. Rossky, K. Johnston, Molecular differences between hydrocarbon and fluorocarbon Surfactants at the CO2/water interface, Journal of Physical Chemistry B, 107 (2003) 10185-10192.
[20] J.Y. Pang, G.Y. Xu, Comparison of the influence of fluorocarbon and hydrocarbon surfactants on the adsorptions of SDS, DTAB and C12E8 at the air/water interface by MD simulation, Chemical Physics Letters, 537 (2012) 118-125.
[21] S.L. Mayo, B.D. Olafson, W.A. Goddard, Dreiding: A generic force field for molecular simulations, J. Phys. Chem., 94 (1990) 8897-8909.
[22] S.S. Jang, S.T. Lin, P.K. Maiti, M. Blanco, W.A. Goddard, P. Shuler, Y.C. Tang, Molecular dynamics study of a surfactant-mediated decane-water interface: Effect of molecular architecture of alkyl benzene sulfonate, Journal of Physical Chemistry B, 108 (2004) 12130-12140.
[23] D. Blunk, R.H. Hetzer, A. Sager-Wiedmann, K. Wirz, Siloxane-containing fire extinguishing foam, in, Universität zu Köln (Cologne), 2017.
[24] J.C. Phillips, R. Braun, W. Wang, J. Gumbart, E. Tajkhorshid, E. Villa, C. Chipot, R.D. Skeel, L. Kale, K. Schulten, Scalable molecular dynamics with NAMD, Journal of Computational Chemistry, 26 (2005) 1781-1802.
[25] B.R. Brooks, C.L. Brooks, A.D. Mackerell, L. Nilsson, R.J. Petrella, B. Roux, Y. Won, G. Archontis, C. Bartels, S. Boresch, A. Caflisch, L. Caves, Q. Cui, A.R. Dinner, M. Feig, S. Fischer, J. Gao, M. Hodoscek, W. Im, K. Kuczera, T. Lazaridis, J. Ma, V. Ovchinnikov, E. Paci, R.W. Pastor, C.B. Post, J.Z. Pu, M. Schaefer, B. Tidor, R.M. Venable, H.L. Woodcock, X. Wu, W. Yang, D.M. York, M. Karplus,

CHARMM: The biomolecular simulation program, Journal of Computational Chemistry, 30 (2009) 1545-1614.
[26] W.a.S.N.S.a.M.B.D. Shi, Molecular simulations of CO2, H2, H2O, and H2S gas absorption into hydrophobic poly(dimethylsiloxane) (PDMS) solvent: solubility and surface tension, The Journal of Physical Chemistry C, 119 (2015) 19253-19265.
[27] T.E. Oliphant, Python for scientific computing, Computing in Science & Engineering, 9 (2007) 10-20.
[28] W. Humphrey, A. Dalke, K. Schulten, VMD: Visual molecular dynamics, Journal of Molecular Graphics, 14 (1996) 33-38.
[29] T. Williams, C. Kelley, Others, Gnuplot 4.2 an interactive plotting program, (2009).
[30] N.B. Vargaftik Handbook of physical properties of liquids and gases, 2 ed., Springer-Verlag Berlin Heidelberg, 1975.
[31] P.L. du Nouy, An interfacial tensiometer for universal use, Journal of General Physiology, 7 (1925) 625-U653.
[32] J. Alejandre, J.L. Rivera, M.A. Mora, V. de la Garza, Force field of monoethanolamine, Journal of Physical Chemistry B, 104 (2000) 1332-1337.
[33] X.H. Zhuang, J.R. Makover, W. Im, J.B. Klauda, A systematic molecular dynamics simulation study of temperature dependent bilayer structural properties, Biochimica Et Biophysica Acta-Biomembranes, 1838 (2014) 2520-2529.
[34] X. Zhuang, E.M. Dávila-Contreras, A.H. Beaven, W. Im, J.B. Klauda, An extensive simulation study of lipid bilayer properties with different head groups, acyl chain lengths, and chain saturations, BBA - Biomembranes, 1858 (2016) 12.
[35] K. Tsujii, Surface activity: principles, phenomena, and applications, 1st ed., Academic Press, San Diego, 1998.
[36] P.K. Yuet, D. Blankschtein, Molecular dynamics simulation study of water surfaces: comparison of flexible water models, Journal of Physical Chemistry B, 114 (2010) 13786-13795.
[37] C. Vega, E. de Miguel, Surface tension of the most popular models of water by using the test-area simulation method, J. Chem. Phys., 126 (2007).
[38] S. Zeppieri, J. Rodriguez, A.L.L. de Ramos, Interfacial tension of alkane plus water systems, Journal of Chemical and Engineering Data, 46 (2001) 1086-1088.
[39] J.L. Rivera, C. McCabe, P.T. Cummings, Molecular simulations of liquid-liquid interfacial properties: Water-n-alkane and water-methanol-n-alkane systems, Physical Review E, 67 (2003).
[40] D. Mitrinovic, A. Tikhonov, M. Li, Z. Huang, M. Schlossman, Noncapillary-wave structure at the water-alkane interface, Physical Review Letters, 85 (2000) 582-585.
[41] C.D. Vecitis, H. Park, J. Cheng, B.T. Mader, M.R. Hoffmann, Enhancement of perfluorooctanoate and perfluorooctanesulfonate activity at acoustic cavitation bubble interfaces, Journal of Physical Chemistry C, 112 (2008) 16850-16857.
[42] J.R. Lu, E.A. Simister, E.M. Lee, R.K. Thomas, A.R. Rennie, J. Penfold, Direct determination by neutron reflection of the penetration of water into surfactant layers at the air/water interface, Langmuir, 8 (1992) 1837-1844.
[43] O. Sonneville-Aubrun, V. Bergeron, T. Gulik-Krzywicki, B. Jonsson, H. Wennerstrom, P. Lindner, B. Cabane, Surfactant films in biliquid foams, Langmuir, 16 (2000) 1566-1579.
[44] O. Belorgey, J.J. Benattar, Structural-properties of soap black films investigated by x-ray reflectivity, Physical Review Letters, 66 (1991) 313-316.
[45] C. Hill, A. Czajka, G. Hazell, I. Grillo, S.E. Rogers, M.W.A. Skoda, N. Joslin, J. Payne, J. Eastoe, Surface and bulk properties of surfactants used in fire-fighting, Journal of Colloid and Interface Science, 530 (2018) 686-694.
[46] F.M. Menger, L. Shi, S.A.A. Rizvi, Re-evaluating the Gibbs analysis of surface tension at the air/Water interface, Journal of the American Chemical Society, 131 (2009) 10380-+.
[47] A.S. Aronson, V. Bergeron, M.E. Fagan, C.J. Radke, The influence of disjoining pressure on foam stability and flow in porous-media, Colloids and Surfaces A, 83 (1994) 109-120.

[48] V. Bergeron, Disjoining pressures and film stability of alkyltrimethylammonium bromide foam films, Langmuir, 13 (1997) 3474-3482.
[49] E. Gorodinsky, S. Efrima, Surface-tension studies of perfluorooctanoate anion in one-component, 2-component, and 3-component systems, Langmuir, 10 (1994) 2151-2158.
[50] M.J. Rosen, Y.F. Wu, Superspreading of trisiloxane surfactant mixtures on hydrophobic surfaces. 1. Interfacial adsorption of aqueous trisiloxane surfactant-N-alkyl pyrrolidinone mixtures on polyethylene, Langmuir, 17 (2001) 7296-7305.
[51] A.I. Rusanov, V.V. Krotov, Manifestation of Gibbs elasticity in thin films, Colloid Journal, 66 (2004) 204-207.
[52] Z.F. Li, A.K. Van Dyk, S.J. Fitzwater, K.A. Fichthorn, S.T. Milner, Atomistic molecular dynamics simulations of charged latex particle surfaces in aqueous solution, Langmuir, 32 (2016) 428-441.
[53] J.A. Davis, R.O. James, J.O. Leckie, Surface ionization and complexation at oxide-water interface .1. Computation of electrical double-layer properties in simple electrolytes, Journal of Colloid and Interface Science, 63 (1978) 480-499.
[54] R. Landauer, Electrical conductivity in inhomogeneous media, American Institute of Physics Conference Proceedings, 40 (1978) 44.
[55] M. Takahashi, zeta potential of microbubbles in aqueous solutions: Electrical properties of the gas-water interface, Journal of Physical Chemistry B, 109 (2005) 21858-21864.
[56] A. Sharipova, S. Aidarova, V.B. Fainerman, A. Stocco, P. Cernoch, R. Miller, Dynamics of adsorption of polyallylamine hydrochloride/sodium dodecyl sulphate at water/air and water/hexane interfaces, Colloids and Surfaces A, 391 (2011) 112-118.
[57] P. Esmaeilzadeh, N. Hosseinpour, A. Bahramian, Z. Fakhroueian, S. Arya, Effect of ZrO2 nanoparticles on the interfacial behavior of surfactant solutions at air-water and n-heptane-water interfaces, Fluid Phase Equilibria, 361 (2014) 289-295.
[58] H. Vatanparast, A. Javadi, A. Bahramian, Silica nanoparticles cationic surfactants interaction in water-oil system, Colloids and Surfaces A, 521 (2017) 221-230.